Article:
Lou, W., Mao, M., Song, K. et al. (12 more authors) (2022) Low permittivity cordierite-based microwave dielectric ceramics for 5G/6G telecommunications. Journal of the European Ceramic Society, 42 (6). pp. 2820-2826. ISSN 0955-2219

https://doi.org/10.1016/j.jeurceramsoc.2022.01.050

Low permittivity cordierite-based microwave dielectric ceramics for 5G/6G telecommunications

Weichao Lou[1], Minmin Mao[1], Kaixin Song[1,*], Kuiwen Xu[1], Bing Liu[1], Wenjun Li[1], Bin Yang[2,*], Zeming Qi[3], Jianwei Zhao[4], Shikuan Sun[5], Huixing Lin[6], Yuanyun Hu[7], Di Zhou[8], Dawei Wang[4,*], and Ian M. Reaney[9,*]

1. College of Electronic Information, Hangzhou Dianzi University, Hangzhou, 310018, China

2.Faculty of Science and Engineering, University of Chester, Chester, CH1 4BJ, UK

3. National Synchrotron Radiation Laboratory, University of Science and Technology of China, Hefei, 230029, China

4. Shenzhen Institute of Advanced Electronic Materials, Shenzhen Institute of Advanced Technology, Chinese Academy of Sciences, Shenzhen, 518055, China

5. School of Material Science and Energy Engineering, Foshan University, Foshan, Guangdong, 528000, China

6. Key Laboratory of Inorganic Functional Material and Device, Shanghai Institute of Ceramics, Chinese Academy of Sciences, Shanghai 200050, China

7. Zhejiang Jiaxing Glead Electronic Co. Ltd., Jiaxing, 314003, China

8.School of Electronic Science and Engineering, Xi'an Jiaotong University, Xi'an, 710049, Shaanxi, China

9. Department of Materials Science and Engineering, University of Sheffield, Sheffield, S1 3JD, UK

Abstract

5G and forthcoming 6G communication systems require dielectric ceramics with low relative permittivity (ε_r) and near-zero temperature coefficient of resonant frequency (τ_f) for the lower part of the microwave (MW) band and at sub-Terahertz. $Mg_2Al_4Si_5O_{18}$ (MAS) ceramics are promising candidates due to their low ε_r (~6) and high-quality factor ($Q\times f$ >40,000 GHz) but have a large τ_f. In this study, 5.5wt% TiO_2 (MAS-$T_{5.5}$) was used to adjust τ_f of MAS to -2.8 ppm/°C whilst retaining low ε_r (5.24) and good $Q\times f$ (33,400 GHz), properties consistent with those obtained by infrared reflectance. A demonstrator microstrip patch antenna with gain 4.92dBi and 76.3% efficiency was fabricated from MAS-$T_{5.5}$.

Keywords: Cordierite; Low permittivity; Terahertz; Patch antenna

1. Introduction

As 5G mobile communication technology develops, the trend is to move towards higher frequency bands, the so-called millimeter wave region, to enable faster data transmission speeds and larger information carrying capacity. 5G and its successor 6G will give birth to the 'internet of things' and enable 'big-data' to be transmitted through the mobile network for the development of smart energy efficient cities and autonomous transport systems. The construction of 5G and 6G base stations will guide the development of new materials, promote artificial intelligence, new concepts in electronics and provide strong support for sustainable growth of the global economy.

Microwave dielectric resonators are widely used in mobile base stations, satellite communications, military radar, global positioning systems (GPS), Bluetooth technology and other engineering fields [1-4] The time delay in a resonator has the following relationship with the relative permittivity (ε_r) [5-6]:

$$t_d = L\frac{\sqrt{\varepsilon_r}}{c} \quad (1)$$

where c represents the velocity of light and L is signal transmission distance. The low time delay of 5G communication therefore requires the dielectric to have a low ε_r and silicate ceramics are consequently important for future millimeter wave technologies [7-10]. Orthorhombic cordierite ($Mg_2Al_4Si_5O_{18}$, MAS) microwave ceramics have low relative permittivity and dielectric loss and were originally reported by Ohsato et al., $\varepsilon_r \approx 6$， $Q\times f \approx 40{,}000$GHz and $\tau_f \approx$ -24 ppm/°C [11-12]. However, its large τ_f and, to a lesser degree, its high sintering temperature (~1400°C) provide potential barriers to commercialization. In previous studies, materials such as $SrTiO_3$[13], $CaTiO_3$[14], TiO_2[15] and Mg_2SiO_4[16] were added to MAS in an attempt to improve MW dielectric properties The most promising results were achieved for composites of $0.75Mg_2Al_4Si_5O_{18}$-$0.25TiO_2$, reported to have τ_f = -0.2 ppm/°C [15], and $(1-x)Mg_2Al_4Si_5O_{18}$-xMg_2SiO_4[16] which reduced the sintering temperature to 1340°C for 50 wt% Mg_2SiO_4, improved $Q\times f$ (76,374 GHz) but had little impact on τ_f (-24 ppm/°C). Although improvements in $Q\times f$ and sintering temperature are important, the primary motivation to facilitate commercialization of MAS is to achieve close to zero τ_f and therefore our study will optimize TiO_2 concentration.

At present, both mobile phones and wireless network cards support a 2.4 GHz

band which passes largely unhindered through masonry in cities. However, its limited bandwidth means that it rapidly becomes crowded, and signals are often dropped when connecting to multiple peripherals. 5.8 GHz transmission is more stable due to fewer consumer devices but requires antennas to work at higher frequencies and thus materials such as MAS with low ε_r are important for current micro- as well as future millimeter wave technology [17-23]. (1-x)$Mg_2Al_4Si_5O_{18}$-xTiO_2 (x = 0-5.5 wt%) microwave ceramics (Abbr. MAS-$T_{x=0-5.5}$) were therefore prepared by solid-state reaction. The effect of TiO_2 concentration on crystal structure, density, and microwave dielectric properties of MAS ceramic were investigated, and a demonstrator 5.8 GHz microstrip patch antenna fabricated.

2 Experimental

2.1 Preparation of MAS-$T_{0-5.5}$ ceramics

High purity raw materials of MgO (99.99%), Al_2O_3 (99.99%), SiO_2 (99.99%) were weighed based on the stoichiometric formula of MAS. Raw materials were ball milled 6 h with ethanol. After drying, mixtures were calcined 4h at 1400℃ to synthesize MAS. TiO_2 (99.99%) with different mass fraction were added into MAS powders and then ball milled. Dried MAS-T slurries were added with 8% PVA as binder, the powders were ground and pressed into cylindrical samples in a steel die at 100 MPa. Finally, the samples were sintered 4h at 1300-1400℃ after burning-out the binder at 600℃.

2.2 Design of MAS-$T_{5.5}$ patch antenna

When the center frequency of the antenna and the relative permittivity of the substrate are clear, the basic size of the patch can be obtained by the following formula [24-25]:

$$W_p = \frac{c}{2f_r}\sqrt{\frac{2}{\varepsilon_r+1}} \tag{2}$$

$$L_p = \frac{c}{2f_r\sqrt{\varepsilon_{eff}}} - 2\Delta L \tag{3}$$

where c represents the speed of light, f_r is the center frequency of the antenna, W_p and L_p are the width and length of the patch, the center frequency f_r is set to 5.8GHz. The effective permittivity ε_{eff}, and correction length ΔL can be calculated by the following equations [26]:

$$\varepsilon_{eff} = \frac{\varepsilon_r+1}{2} + \frac{\varepsilon_r-1}{2\sqrt{1+12h/W_p}} \tag{4}$$

$$\Delta L = 0.412h\frac{(\varepsilon_{eff}+0.3)\left({}^{W_p}/_{h}+0.264\right)}{(\varepsilon_{eff}-0.258)\left({}^{W_p}/_{h}+0.8\right)} \tag{5}$$

where h is the thickness of the ceramic substrate. CST 2020 software was used to simulate the antenna prototype to get the final patch size.

2.3 Manufacture of MAS-$T_{5.5}$ patch antenna

With the help of adding 5 wt% PVA, MAS-$T_{5.5}$ powder was pressed into a 2 mm thick sample by a 20 mm× 20 mm custom-made mold, which was sintered 6 hours at 1350℃ to obtain ceramic substrate. Using dimensions predicted by the CST simulation, double-sided conductive copper foil was cut and adhered to the ceramic substrate with a SubMiniature version A(SMA) connector soldered onto the patch to connect the

ground plane and surface electrode.

2.4 Characterization

Crystal structure was analyzed on crushed and ground ceramic powders with a Rigaku, SmartLab9KW, X-ray diffractometer (XRD) using Cu $K\alpha$ radiation. Powder X and FullProf software were used to refine the XRD data to obtain the crystal structure and lattice parameters. After polishing and thermal etching at a temperature of 150°C lower than the sintering temperature for 1 hour, the surface microstructures of sintered ceramics were observed by scanning electron microscopy (SEM, JEOL, JSM-1T500HR) and the elemental composition was analyzed by energy dispersive spectrometer (EDS). Raman spectra was obtained by 2 mm thick samples and a LabRAM HR800 spectrometer operated with a 532 nm laser. Infrared reflectance spectra were collected with 2 mm thick samples on the IFS 66v/S beam line of the Hefei National Synchrotron Radiation Laboratory. 5-6 mm thick ceramic samples were measured on an Agilent E8362B network analyzer using the TE01δ mode dielectric resonator method to obtain the ε_r and $Q\times f$ values. τ_f was obtained using equation (6):

$$\tau_f = \frac{f_2 - f_1}{f_1 \times (T_2 - T_1)} \times 10^6 \quad (6)$$

where f_1 and f_2 are the resonant frequency at 25°C and 85°C, respectively. The dielectric properties at THz frequencies were measured using a THz-TDS (THz time-domain spectroscopy) system (from TeTechs Ltd). Thin polished plane-parallel specimens were measured from 0.2 THz to 2 THz in transmission mode to obtain the permittivity and loss tangents [27].

The reflection coefficient S11 of the patch antenna was obtained using a network analyzer (N5234B, Keysight) and its efficiency and radiation pattern in the far field determined in a microwave anechoic chamber (SATIMO SG24).

3 Results and discussion

The bulk density of MAS-$T_{0\text{-}5.5}$ ceramics at different sintering temperatures are shown in Figure 1. The optimal sintering temperature decreases with the increase in fraction of TiO_2. The maximum bulk density of MAS-$T_{5.5}$ is 2.481g/cm^3 at 1320°C which corresponded to a relative density of 95%.

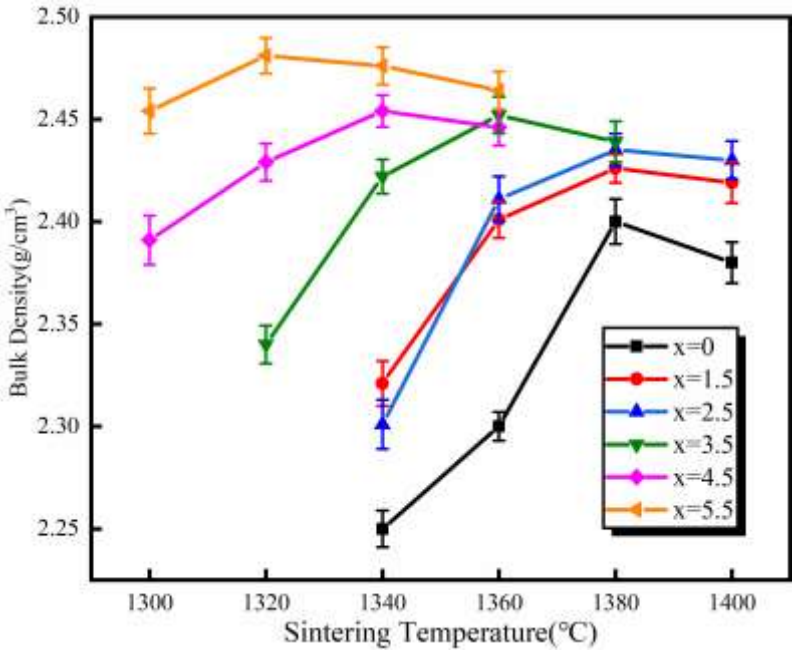

Figure 1. The bulk density of MAS-$T_{0\text{-}5.5}$ ceramics as a function of sintering temperature.

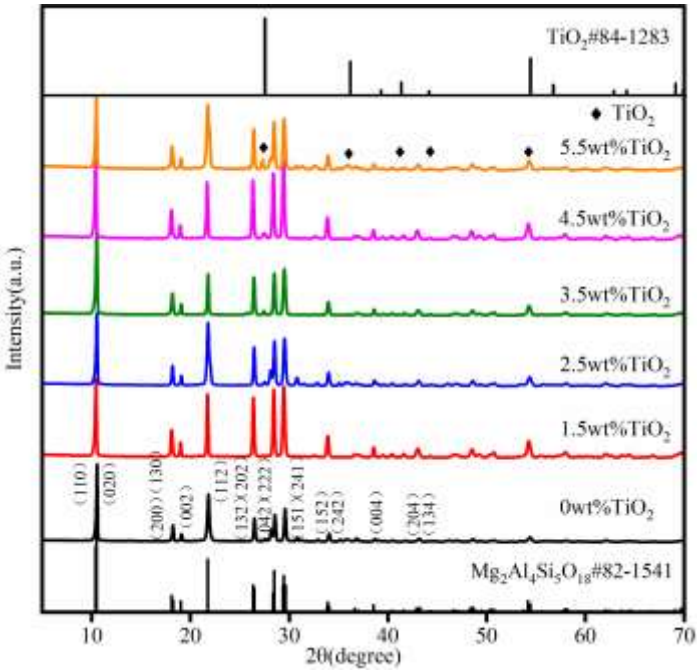

Figure 2. XRD patterns of MAS-$T_{0\text{-}5.5}$ ceramics.

Figure 2 displays the XRD patterns of MAS-xT ceramics. When x=0, the diffraction peaks correspond to the $Mg_2Al_4Si_5O_{18}$ cordierite phase (JCPDS No.82-1541) with a space group of *Cccm* (66). As x increases, diffraction peaks of TiO_2 are simultaneously observed alongside those of the cordierite phase. XRD data from MAS-$T_{5.5}$ were refined to determine the concentration of Ti in the cordierite structure, Table S1 (Supporting Information) and Figure 3a. Refinements indicate that Ti is most likely to occupy the Si3 position in the cordierite phase, and that the weight fractions of MAS and TiO_2 are 95.72% and 4.28%, respectively, which suggests that only a small concentration of TiO_2 (~1%) resides within the MAS. The refined structure parameters of MAS and TiO_2 are listed in Table S2 and Table S3 (Supporting Information). The orthorhombic crystal structure of MAS is shown in Figure 3b (a-b plane) and Figure 3c (a-c plane). MAS has a layered structure, in which [Mg_6] hexagons are connected by

[AlO_4] and [SiO_4] tetrahedra, with [Al_2Si_4] hexagons connected by O atoms. The crystal structure of rutile TiO_2 is shown in Figure 3d.

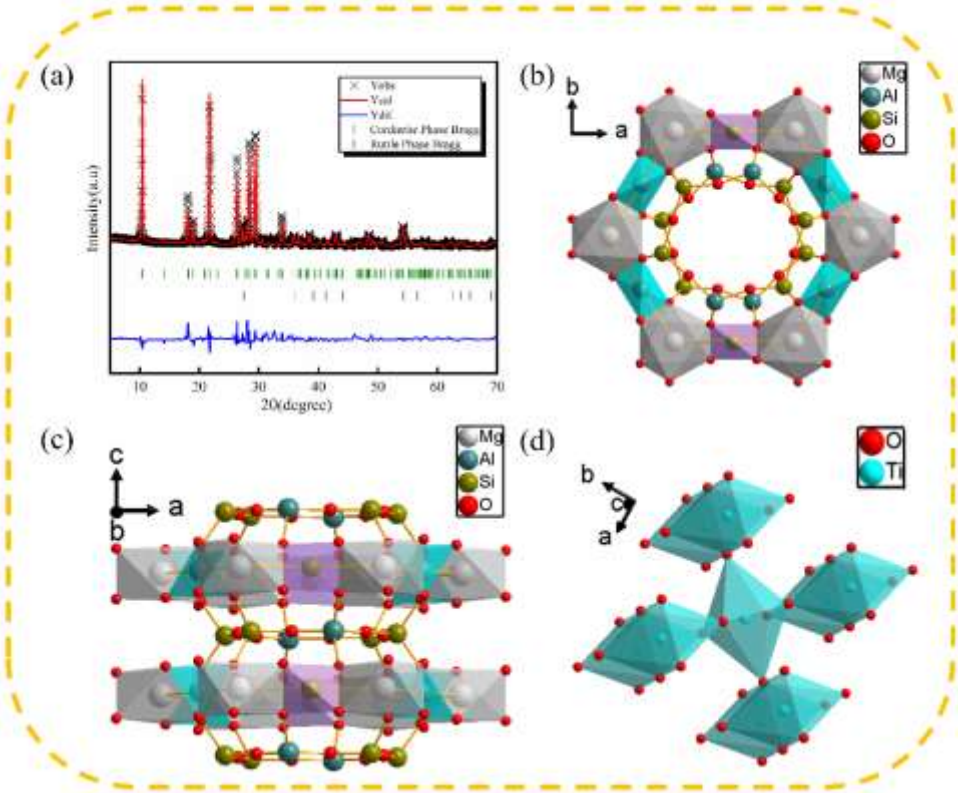

Figure 3. (a) Rietveld refinement of MAS-$T_{5.5}$ ceramic. (b-c) The crystal structure schematics of MAS on the a-b plane and a-c plane. (d) Schematic of rutile TiO_2.

The SEM images of MAS-T_x (x = 1.5, 2.5, 5.5) ceramics sintered at the optimal sintering temperature are shown in Figure 4a-c, the corresponding grain distribution displayed in Figure 4d-f. It is observed that the average grain size of MAS-T ceramics decreases from 1.19 μm to 1.09 μm, which suggests that the addition of TiO_2 inhibits the grain growth of MAS. The standard deviation of grain size distribution correspondingly decreases, indicating that the grain size distribution gradually becomes uniform. Meanwhile, the EDS elemental mapping results are given in Figure S1

(Supporting Information), which show that the distribution of TiO_2 is random and uniform in MAS host.

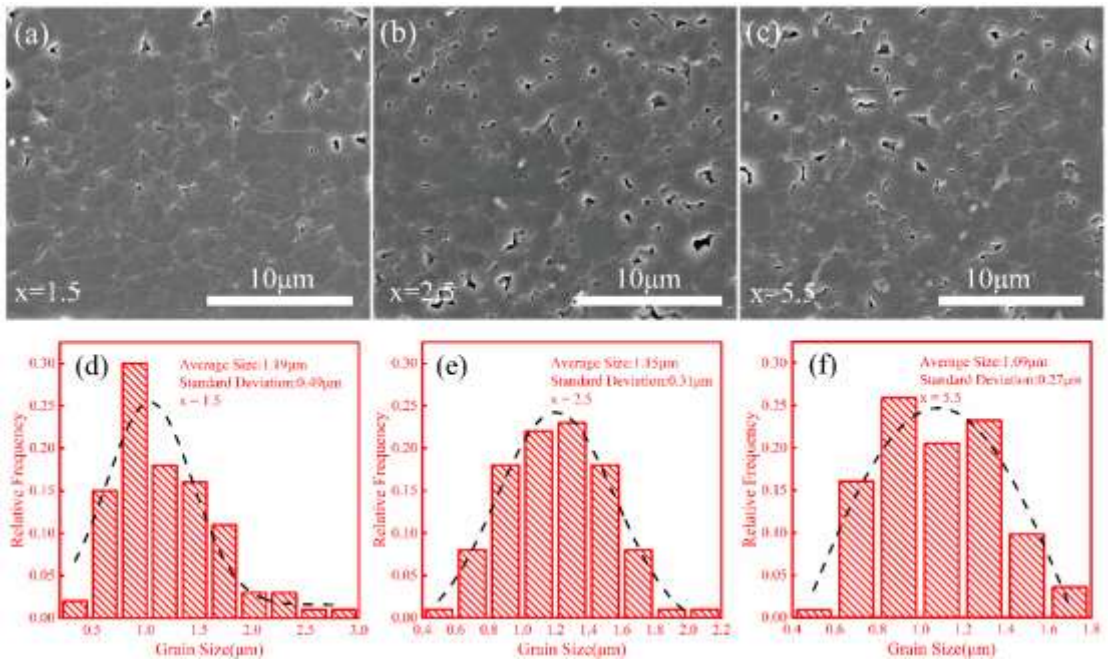

Figure 4. SEM images of the polished and thermal etched surfaces of MAS-T_x ceramics (a) x = 1.5, (b) x = 2.5, (c) x = 5.5; The grain size distribution of MAS-T_x ceramics (d) x = 1.5, (e) x = 2.5, (f) x = 5.5.

The microwave dielectric properties of MAS-$T_{0\text{-}5.5}$ ceramics are shown in Figure 5. With the increase of TiO_2 concentration, ε_r increases from 4.63 to 5.24 which is attributed to the enhanced density of composite ceramics and the higher ε_r of TiO_2[28-29]. The $Q\times f$ of the MAS is 50,560GHz but increases to 61,720GHz for x=1.5, indicating that in small concentrations, TiO_2 can reduce dielectric loss (tanδ). τ_f of MAS is tuned close to zero (-2.8ppm/°C) with x = 5.5, due to the positive τ_f of TiO_2. Table 1 lists the recently reported properties of composite ceramics. It should be noted that the MAS-$T_{5.5}$ ceramic in this work has a smaller ε_r and a relatively high $Q\times f$ value [30-34].

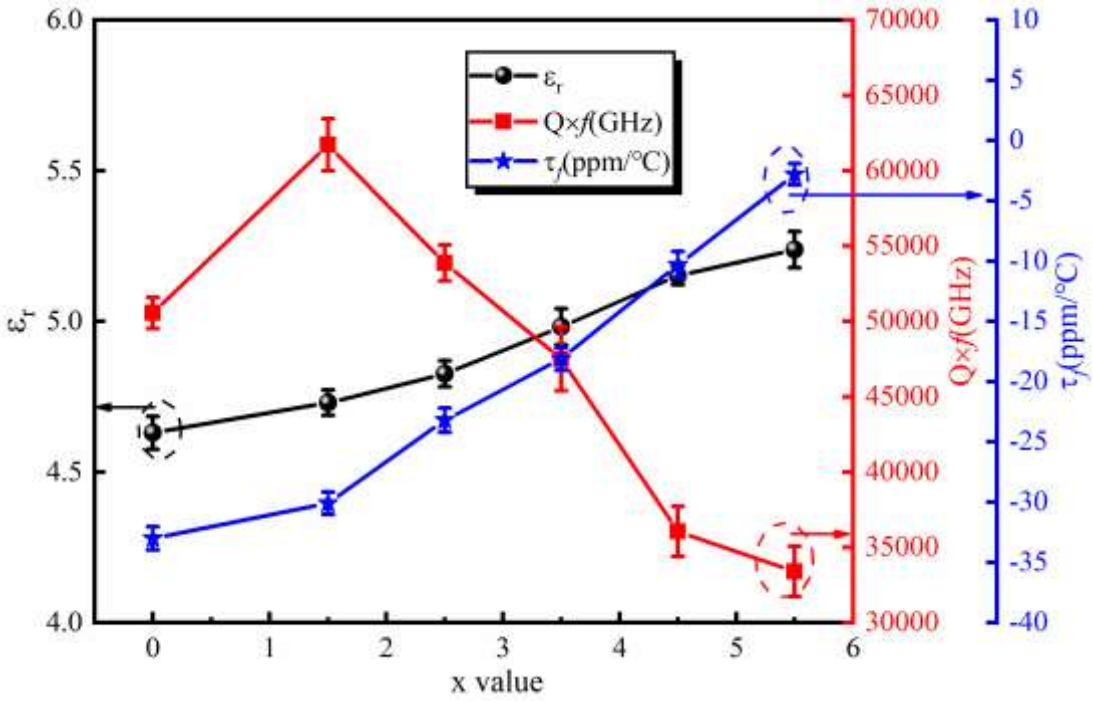

Figure 5. Microwave dielectric properties of MAS-$T_{0\text{-}5.5}$ ceramics as a function of TiO_2 weight fraction.

Table 1. Comparison of microwave dielectric properties at terahertz band.

Composition	ε_r	Q×*f*(GHz)	Ref
$(Ba_{0.2}Sr_{0.8})_{0.75}La_{4.25}Ti_{3.75}Al_{0.25}O_{15}$	45	~100,000@1THz	[30]
$La_2Ti_2O_7$	27	~10,000@1THz	[31]
$Sm(Nb_{0.7}V_{0.3})O_4$	20	~10,000@1THz	[32]
$Co_{0.5}Sn_{0.5}TaO_4$	16	~80,000@1THz	[33]
Zn_2SiO_4	6	~200,000@1THz	[34]
$Mg_2Al_4Si_5O_{18}$-5.5 wt%TiO_2	4.5	~160,000@1THz	This work

Lattice vibration modes and crystal structure of microwave dielectric ceramic are often analyzed by Raman spectroscopy[35-38]. The cordierite structure with *Cccm* symmetry has 174 vibrational modes derived from the group theoretical calculations:

$$\Gamma = 23A_g + 25B_{1g} + 19B_{2g} + 20B_{3g} +$$

$$17A_u + 19B_{1u} + 25B_{2u} + 26B_{3u} \quad (7)$$

where 87 g-modes are Raman-active; 67 u-modes are IR-active, 17 A_u-modes are inactive [39]. The Raman spectra of MAS-$T_{0\text{-}5.5}$ ceramics are shown in Figure 6a. The peaks at 554 cm^{-1} and 576 cm^{-1} correspond to the stretching vibration of Mg-O bond, which are affected by the Ti-O bond and their relative strength gradually weakens as shown in Figure 6b. The origin of 121 cm^{-1} and 154 cm^{-1} peaks are bending vibrations of the Si-O bond, the peaks at 971 cm^{-1}, 1008 cm^{-1} and 1191 cm^{-1} are stretching vibrations of the Si-O bond and the peaks at 295 cm^{-1} and 674 cm^{-1} are related to the stretching vibration of the Al-O bond [40-42]. All Raman bands belong to either MAS or TiO_2 as shown in Fig 6b, indicating the coexistence of MAS and TiO_2, consistent with the XRD and SEM results.

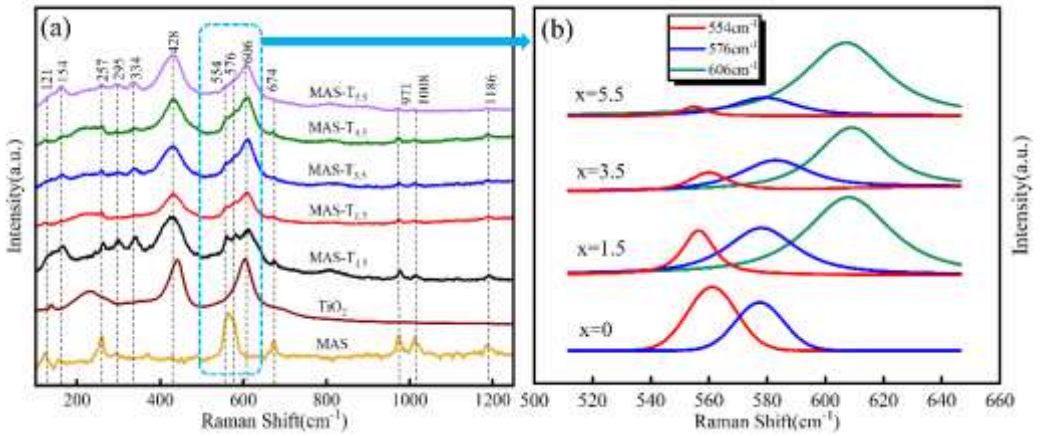

Figure 6. (a) Raman spectra of MAS-$T_{0\text{-}5.5}$ ceramics. (b) Raman peak splitting results at 500-660cm^{-1}.

ε_r and tanδ of MAS-T_x(x=0, 1.5, 5.5) ceramics from 0.2 THz to 2 THz are shown in Fig. 7a,b. ε_r in the THz band is smaller than that at microwave frequencies, which is

attributed to intrinsic factors such as dipoles and lattice vibrations. The intrinsic microwave dielectric properties of MAS-T_x (x=0, 1.5, 5.5) ceramics were further investigated by infrared reflectance, and the results analyzed using a classical harmonic oscillator model[43-47]:

$$R(\omega) = \left|\frac{\sqrt{\varepsilon^*(\omega)}-1}{\sqrt{\varepsilon^*(\omega)}+1}\right|^2 \quad (8)$$

$$\varepsilon^*(\omega) = \varepsilon'(\omega) - i\varepsilon''(\omega) = \varepsilon_\infty + \sum_{j=1}^{n} \frac{S_j}{\omega_j^2 - \omega^2 + i\omega\gamma_j} \quad (9)$$

where ε_∞ represents the optical permittivity produced by electron polarization, n is the number of active optical modes, S_j, ω_j and γ_j are the plasma frequency, eigenfrequency and damping constant of the j-th mode, respectively. Further we can obtain the imaginary and real parts of the dielectric constant:

$$\varepsilon'(\omega) = \varepsilon_\infty + \sum_{j=1}^{n} \frac{S_j(\omega_j^2 - \omega^2)}{(\omega_j^2 - \omega^2)^2 + \omega^2 r_j^2} \quad (10)$$

$$\varepsilon''(\omega) = \sum_{j=1}^{n} \frac{S_j \omega r_j}{(\omega_j^2 - \omega^2)^2 + \omega^2 r_j^2} \quad (11)$$

The infrared reflection spectrum, fitted using 17 modes (Table S6, Supporting Information; Figure 7c), and the complex dielectric constants of MAS-$T_{5.5}$ ceramic are shown in Figure 7c-d. The 171.57cm^{-1} mode at 29.6% has the highest contribution to tanδ. The dielectric properties measured in the microwave and the THz band are marked by black circles and blue triangles, respectively. Compared with x = 0 and 1.5 (Figure S2, Supporting Information), the calculated ε_r and tanδ are in good agreement with the measured results for x = 5.5, indicating that the dielectric properties of MAS-T_x (x=0, 1.5, 5.5) ceramics mostly arise from lattice vibration and ion displacement polarization.

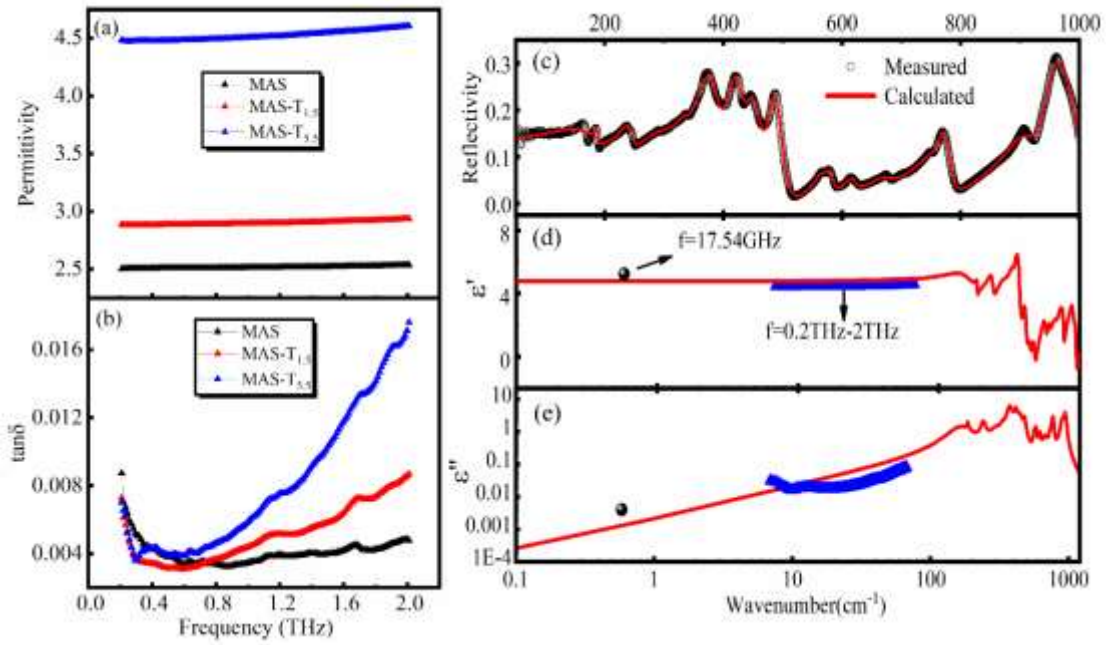

Figure 7. (a-b) The permittivity and tanδ of MAS-T_x(x=0, 1.5, 5.5) ceramics at 0.2THz-2THz. (c) Experimental and fitted infrared reflectance spectra of MAS-$T_{5.5}$ ceramic. (d-e) The complex dielectric constants of MAS-$T_{5.5}$ ceramic.

With the rapid development of wireless communication technology, antennas have received widespread attention as a key device for signal transmission and reception [48-50]. MAS-$T_{5.5}$ ceramics have a low ε_r and near-zero τ_f, and are thus promising candidates for 5G/6G technology. MAS-$T_{5.5}$ was chosen as the substrate to fabricate patch antennas aiming for the Sub-6GHz. The initial size of the patch is calculated by the above formula of (2)-(5) in experimental part, where h is the thickness of the ceramic substrate and the center frequency f_r is set to 5.8GHz. The dimensions of the ceramic substrate and patch obtained by simulation are displayed in Figure 8a. The size of MAS-$T_{5.5}$ substrate is 17mm × 17mm × 1.15mm, the length and width of the patch are 11.1mm and 14.9mm, respectively. Figure 8b also provides a picture of the antenna being

measured in the microwave anechoic chamber. In general, the reflection coefficient (S_{11}) of the antenna indicates the amount of energy reflected. The simulated and measured S_{11} of the patch antenna at various frequencies are shown in Figure 8c. The experimental S_{11} results illustrate that the center frequency and bandwidth are 5.86 GHz and 120 MHz, in keeping with the simulated results. The simulated and measured radiation pattern at 5.86 GHz after normalization is plotted in Figure 8 d, e, with similar patterns on the E (phi = 0) and H planes (phi = 90). The antenna has good radiation characteristics and its radiation direction is perpendicular to the patch. Moreover, the angular width of 3dB is about 88° from the E plane, which is close to 96.6° obtained by simulation. The patch antenna is biased toward the directional radiation mode, and the maximum radiation direction is at 0°. The simulated and measured gain and efficiency of the antenna are shown in Figure 8f. The measured gain at 5.86GHz is 4.92dBi, indicating that the patch antenna has good directivity at the operating frequency. The maximum efficiency of the antenna is 85.2% at 5.79 GHz, while the maximum efficiency of the simulation is 68%, and the efficiency at 5.86 GHz is 76.3%. The efficiency of Wi-Fi antennas in electronic products is usually around 70%[51-52] and therefore, patch antennas based on MAS-$T_{5.5}$ are considered suitable for 5 GHz Wi-Fi antenna applications.

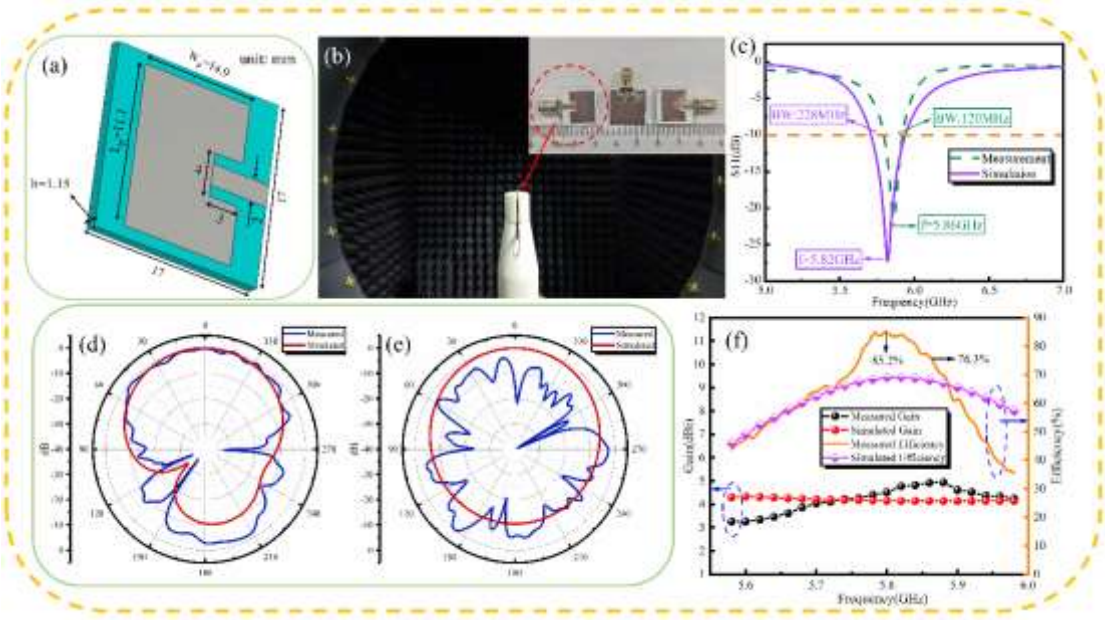

Figure 8. (a) The dimensions of antenna substrate and patch. (b) The microwave anechoic chamber system. (c) Simulated and experimental S_{11} of the patch antenna. (d) Simulated and measured radiation pattern at E plane. (e) Simulated and measured radiation pattern at H plane. (f) Simulated and measured gain and efficiency.

4 Conclusions

In this work, the τ_f of MAS based ceramics is optimized by forming a composite with TiO_2. The XRD, SEM and Raman spectra results illustrate that the MAS and TiO_2 coexist but Rietveld refinement indicates partial interaction in which ~1%wt of TiO_2 diffuses into the MAS lattice, with Ti preferentially occupying Si3 positions. Temperature stable composites are achieved for x = 5.5 with $\varepsilon_r = 5.24$，$Q \times f = 33{,}400$ GHz and $\tau_f = -2.8$ ppm/°C. Patch antennas based on MAS-$T_{5.5}$ ceramic substrates were fabricated with a measured center frequency of 5.86 GHz with S_{11} -22.76 dB and bandwidth of 120 MHz at -10 dB, in good agreement with the simulations. The radiation

pattern at 5.86GHz demonstrates good antenna characteristics with excellent gain (4.92dBi) and efficiency (76.3%) at center frequency, indicating that the MAS-$T_{5.5}$ patch antennas are suitable for 5 GHz Wi-Fi applications.

Acknowledgements

This work was supported by the National Natural Science Foundation of China under Grant No. 52161145401&51672063. Professor Reaney would like to acknowledge the support of Engineering and Physical Science Research Council under Grant No. EP/V026402/1. K. Song also acknowledges the Guangdong Key Platform & Programs of the Education Department of Guangdong Province for funding under Grant No. 2021ZDZX1003.

Declaration of competing interest

The authors declare that they have no known competing financial interests or personal relationships that could have appeared to influence the work reported in this paper.

References

[1] I. M. Reaney, D. Iddles, Microwave dielectric ceramics for resonators and filters in mobile phone networks, J. Am. Ceram. Soc. 89 (2006) 2063-2072.

[2] F. Liu, J. Guo, L. Zhao, X. Shen, Y. Yin, A meta-surface decoupling method for two linear polarized antenna array in Sub-6 GHz base station applications, IEEE Access. 7 (2019) 2759-2768.

[3] Y. Zhan, L. X. Li, Low-permittivity and high-Q value $Li_2Mg_3Ti_{1-x}(Zn_{1/3}Nb_{2/3})_xO_6$ microwave dielectric ceramics for microstrip antenna applications in 5G millimeter wave, J. Alloys Compd. 857 (2021) 157608.

[4] D. W. Wang, B. Siame, S. Y. Zhang, G. Wang, X. S. Ju, L. H. Li, Z. L. Lu, Y. Vardaxoglou, W. Whittow, D. Cadman, S. K. Sun, D. Zhou, K. X. Song, I. M. Reaney, Direct integration of cold sintered, temperature-stable $Bi_2Mo_2O_9$-K_2MoO_4 ceramics on printed circuit boards for satellite navigation antennas, J. Eur. Ceram. Soc. 40 (2020) 4029-4034.

[5] B. Liu, X. Q. Liu, X. M. Chen, $Sr_2LaAlTiO_7$: a new ruddlesden-popper compound with excellent microwave dielectric properties, J. Mater. Chem. C. 4 (2016) 1720-1726.

[6] L. X. Pang, D. Zhou, Z. M. Qi, W. G. Liu, Z. X. Yue, I. M. Reaney, Structure-property relationships of low sintering temperature scheelite-structured (1-x)$BiVO_4$-x$LaNbO_4$ microwave dielectric ceramics, J. Mater. Chem. C. 5 (2017) 2695-2701.

[7] C. X. Su, L. Y. Ao, Z. W. Zhang, Y. F. Zhai, J. Q. Chen, Y. Tang, L. J. Liu, L. Fang, Crystal structure, Raman spectra and microwave dielectric properties of novel temperature-stable $LiYbSiO_4$ ceramics, Ceram. Int. 46 (2020) 19996-20003.

[8] H. Ohsato, T. Tsunooka, T. Sugiyama, K. Kakimoto, H. Ogawa, Forsterite ceramics for millimeterwave dielectrics, J. Electroceram. 17 (2006) 445-450.

[9] I. J. Induja, M. T. Sebastian, Microwave dielectric properties of mineral sillimanite obtained by conventional and cold sintering process, J. Eur. Ceram. Soc. 37 (2017)

2143-2147.

[10] X. Q. Song, W. Z. Lu, Y. H. Lou, T. Chen, S. W. Ta, Z. X. Fu, W. Lei, Synthesis, lattice energy and microwave dielectric properties of $BaCu_{2-x}Co_xSi_2O_7$ ceramics, J. Eur. Ceram. Soc. 40 (2020) 3035-3041.

[11] M. Terada, K. Kawamura, I. Kagomiya, K. Kakimoto, H. Ohsato, Effect of Ni substitution on the microwave dielectric properties of cordierite, J. Eur. Ceram. Soc. 27 (2007) 3045-3048.

[12] H. Ohsato, I. Kagomiya, M. Terada, K. Kawamura, Origin of improvement of Q based on high symmetry accompanying Si-Al disordering in cordierite millimeter-wave ceramics, J. Eur. Ceram. Soc. 30 (2010) 315-318.

[13] K. X. Song, S. Wu, P. Liu, H. X. Lin, Z. H. Ying, P. Zheng, W. T. Su, J. X. Deng, L. Zheng, H. B. Qin, Phase composition and microwave dielectric properties of $SrTiO_3$ modified $Mg_2Al_4Si_5O_{18}$ cordierite ceramics, J. Alloys Compd. 628 (2015) 57-62.

[14] J. S. Wei, P. Liu, H. X. Lin, Z. H. Ying, P. Zheng, W. T. Su, K. X. Song, H. B. Qin, Crystal structure and microwave dielectric properties of $CaTiO_3$ modified $Mg_2Al_4Si_5O_{18}$ cordierite ceramics, J. Alloys Compd. 689 (2016) 81-86.

[15] S. Wu, K. X. Song, P. Liu, H. X. Lin, F. F. Zhang, P. Zheng, H. B. Qin, Effect of TiO_2 doping on the structure and microwave dielectric properties of cordierite ceramics, J. Am. Ceram. Soc. 98 (2015) 1842-1847.

[16] X. Dong, C. L. Sun, H. Y. Yang, L. Y. Yang, S. R. Zhang, Influence of Mg_2SiO_4 addition on crystal structure and microwave properties of $Mg_2Al_4Si_5O_{18}$ ceramic

system. J. Mater. Sci.: Mater. Electron, 29 (2018) 17967-17973.

[17] A. Ullah, H. X. Liu, A. Manan, A. S. Ahmad, P. C. Zhai, H. Hao, M. H. Cao, Z. H. Yao, A. Ullah, A. Jan, M. Emmanuel, J. Iqbal, Microwave dielectric properties of $Bi_2(Li_{0.5}Ta_{1.5})O_7$-$TiO_2$-based ceramics for 5G cellular base station resonator application, Ceram. Int. 47 (2021) 8416-8423.

[18] S. Wang, W. J. Luo, L. X. Li, M. K. Du, J. L. Qiao, Improved tri-layer microwave dielectric ceramic for 5G applications, J. Eur. Ceram. Soc. 41 (2021) 418-423.

[19] S. H. Yoon, G. K. Choi, D. W. Kim, S. Y. Cho, K. S. Hong, Mixture behavior and microwave dielectric properties of (1-x)$CaWO_4$-xTiO_2, J. Eur. Ceram. Soc. 27 (2007) 3087-3091.

[20] D. W. Kim, K. H. Ko, D. K. Kwon, K. S. Hong, Origin of microwave dielectric loss in $ZnNb_2O_6$-TiO_2, J. Am. Ceram. Soc. 85 (2002) 1169-1172.

[21] J. Guo, D. Zhou, H. Wang, X. Yao, Microwave dielectric properties of (1-x)$ZnMoO_4$-xTiO_2 composite ceramics, J. Alloys Compd. 509 (2011) 2863-2865.

[22] L. X. Pang, H. Wang, D. Zhou, X. Yao, A new temperature stable microwave dielectric with low-firing temperature in Bi_2MoO_6-TiO_2 system, J. Alloys Compd. 493 (2010) 626-629.

[23] Z. Y. Tan, K. X. Song, H. B. Bafrooei, B. Liu, J. Wu, J. M. Xu, H. X. Lin, D. W. Wang, The effects of TiO_2 addition on microwave dielectric properties of $Y_3MgAl_3SiO_{12}$ ceramic for 5G application, Ceram. Int. 46 (2020) 15665-15669.

[24] Y. P. Ji, K. X. Song, S. Y. Zhang, Z. L. Lu, G. Wang, L. H. Li, D. Zhou, D. W. Wang, I. M. Reaney, Cold sintered, temperature-stable $CaSnSiO_5$-K_2MoO_4 composite

microwave ceramics and its prototype microstrip patch antenna, J. Eur. Ceram. Soc. 41 (2021) 424-429.

[25] H. C. Xiang, J. Kilpijarvi, S. Myllymaki, H. T. Yang, L. Fang, H. Jantunen, Spinel-olivine microwave dielectric ceramics with low sintering temperature and high quality factor for 5 GHz Wi-fi antennas, Appl. Mater. Today. (2021) 100826.

[26] P. Ramachandran, H. Kahari, J. Juuti, H. Jantunen, Room temperature densified ceramics for weight optimized circular polarized GPS antenna design, Microw. Opt. Techno. Lett. 60 (2018) 1061-1066.

[27] Y. Zeng, M. Edwards, R. Stevens, J. Bowen, R. S. Donnan, B. Yang, Terahertz characterization of UV offset lithographically printed electronic-ink, Organic Electronics. 48 (2017) 382-388.

[28] Z. Y. Tan, K. X. Song, H. B. Bafrooei, et al. The effects of TiO_2 addition on microwave dielectric properties of $Y_3MgAl_3SiO_{12}$ ceramic for 5G application. Ceram. Int. 46(2020) 15665-15669.

[29] X. C. Lu, W. J. Bian, B. Quan, et al. Compositional tailoring effect on $ZnGa_2O_4$-TiO_2 ceramics for tunable microwave dielectric properties. J. Alloys Compd. 792(2019) 742-749.

[30] Y. Luo, W, J. Guo, Y. G. Chen, J. Zhang, Z. X. Yue, Thermally-stimulated defect relaxations and microwave/terahertz dielectric response of La,Al co-doped $(Ba,Sr)La_4Ti_4O_{15}$ ceramics, J. Eur. Ceram. Soc. 41 (2021) 158-164.

[31] M. Zhang, Z. Y. Tang, H. F. Zhang, G. Smith, Q. H. Jiang, T Saunders, B. Yang, H. X. Yan, Characterization of microwave and terahertz dielectric properties of single

crystal $La_2Ti_2O_7$ along one single direction, J. Eur. Ceram. Soc. 41 (2021) 7375-7379.

[32] F. F. Wu, D. Zhou, C. Du, S. K. Sun, L. X. Pang, B. B. Jin, Z. M. Qi, J. Varghese, Q. Li, X. Q. Zhang, Temperature stable $Sm(Nb_{1-x}V_x)O_4$ ($0.0 \leq x \leq 0.9$) microwave dielectric ceramics with ultra-low dielectric loss for dielectric resonator antenna applications, J. Mater. Chem. C. 9 (2021) 9962.

[33] H. Yang, P. Wu, M. Xing, E. Li, L. Chai , Structure, microwave dielectric properties, and THz spectrum of $Co_{0.5}Sn_{0.5}TaO_4$ ceramics. Mater. Lett. 306 (2022) 130917.

[34] B. Synkiewicz-Musialska, D. Szwagierczak, J. Kulawik, N. Pałka, P. R. Bajurko, Impact of additives and processing on microstructure and dielectric properties of willemite ceramics for LTCC terahertz applications, J. Eur. Ceram. Soc. 40 (2020) 362-370.

[35] Y. Y. Wang, J. Q. Lv, E. C. Xiao, Z. M. Qi, Z. X. Yue, Y. Chen, G. H. Chen, F. Shi, Internal relations between crystal structures and dielectric properties of (1-x)$BaWO_4$-xTiO_2 composite ceramics, J. Mater. Sci.: Mater. Electron. 31 (2020) 19961-19973.

[36] K. Cheng, C. C. Li, C. Z. Yin, Y. Tang, Y. H. Sun, L. Fang, Effects of Sr^{2+} substitution on the crystal structure, Raman spectra, bond valence and microwave dielectric properties of $Ba_{3-x}Sr_x(VO_4)_2$ solid solutions, J. Eur. Ceram. Soc. 39 (2019**)** 3738-3743.

[37] H. Y. Yang, S. R. Zhang, Y. W. Chen, H. C. Yang, Y. Yuan, E. Z. Li, Crystal chemistry, Raman spectra, and bond characteristics of trirutile-type $Co_{0.5}Ti_{0.5}TaO_4$

microwave dielectric ceramics, Inorg. Chem. 58 (2019) 968-976.

[38] Q. B. Lin, K. X. Song, B. Liu, H. B. Bafrooei, D. Zhou, W. T. Su, F. Shi, D. W. Wang, H. X. Lin, I. M. Reaney, Vibrational spectroscopy and microwave dielectric properties of $AY_2Si_3O_{10}$ (A = Sr, Ba) ceramics for 5G applications, Ceram. Int. 46 (2020) 1171-1177.

[39] R. Kaindl, D. M. Tobbens, U. Haefeker, Quantum-mechanical calculations of the Raman spectra of Mg- and Fe-cordierite, Am. Mineral. 96 (2011) 1568-1574.

[40] A. Y. Likhacheva, S. V. Goryainov, A. S. Krylov, T. A. Bulbak, P. S. R. Prasad, Raman spectroscopy of natural cordierite at high water pressure up to 5 Gpa, J. Raman. Spectrosc. 43 (2012) 559-563.

[41] K. X. Song, P. Liu, H. X. Lin, W. T. Su, J. Jiang, S. Wu, J. Wu, Z. H. Ying, H. B. Qin, Symmetry of hexagonal ring and microwave dielectric properties of $(Mg_{1-x}Ln_x)_2Al_4Si_5O_{18+x}$(Ln = La, Sm) cordierite-type ceramics, J. Eur. Ceram. Soc. 36 (2016) 1167-1175.

[42] C. Xing, J. Z. Li, J. Wang, H. L. Chen, H. Y. Qiao, X. Q. Yin, Q. Wang, Z. M. Qi, F. Shi, Internal relations between crystal structures and intrinsic properties of nonstoichiometric $Ba_{1+x}MoO_4$ ceramics, Inorg. Chem. 57 (2018) 7121-7128.

[43] H. H. Guo, D. Zhou, W. F. Liu, L. X. Pang, D. W. Wang, J. Z. Su, Z. M. Qi, Microwave dielectric properties of temperature-stable zircontype (Bi,Ce)VO_4 solid solution ceramics, J. Am. Ceram. Soc. 103 (2019) 423-431.

[44] D. Zhou, D. Guo, W. B. Li, L. X. Pang, X. Yao, D. W. Wang, I. M. Reaney, Novel temperature stable high-ε_r microwave dielectrics in the Bi_2O_3-TiO_2-V_2O_5 system.

J. Mater. Chem. C. 4 (2016) 5357-5362.

[45] D. Zhou, L. X. Pang, D. W. Wang, C. Li, B. B. Jin, I. M. Reaney, High permittivity and low loss microwave dielectrics suitable for 5G resonators and low temperature co-fired ceramic architecture, J. Mater. Chem. C. 5 (2017) 10094-10098.

[46] J. Q. Chen, Y. Tang, C. Z. Yin, M. Y. Yu, H. C. Xiang, C. C. Li, X. R. Xiang, L. Fang, Structure, microwave dielectric performance, and infrared reflectivity spectrum of olivine-type $Mg_2Ge_{0.98}O_4$ ceramic, J. Am. Ceram. Soc. 103 (2019) 1789-1797.

[47] H. H. Guo, M. S. Fu, D. Zhou, C. Du, P. J. Wang, L. X. Pang, W. F. Liu, A. S. B. Sombra, J. Z. Su, Design of a high-efficiency and gain antenna using novel low-loss, temperature-stable $Li_2Ti_{1-x}(Cu_{1/3}Nb_{2/3})_xO_3$ microwave dielectric ceramics, ACS Appl. Mater. Inter. 13 (2021) 912-923.

[48] H. H. Guo, D. Zhou, C. Du, P. J. Wang, W. F. Liu, L. X. Pang, Q. P. Wang, J. Z. Su, C. Singh, S. Trukhanov, Temperature stable $Li_2Ti_{0.75}(Mg_{1/3}Nb_{2/3})_{0.25}O_3$-based microwave dielectric ceramics with low sintering temperature and ultra-low dielectric loss for dielectric resonator antenna applications, J. Mater. Chem. C. 8 (2020) 4690-4700.

[49] C. Du, H. H. Guo, D. Zhou, H. T. Chen, J. Zhang, W. F. Liu, J. Z. Su, H. W. Liu, Dielectric resonator antennas based on high quality factor $MgAl_2O_4$ transparent dielectric ceramics, J. Mater. Chem. C. 8 (2020) 14880-14885.

[50] M. H. Ullah, M. T. Islam, Design of a modified W-shaped patch antenna on Al_2O_3 ceramic material substrate for Ku-band, Chalcogenide. Lett. 9 (2012) 61-66.

[51] D. E. Bockelman, W. R. Eisenstadt, Combined differential and common-mode scattering parameters: theory and simulation, IEEE T. Micro. Theory. 43 (1995) 1530-1539.

[52] D. C. Thompson, O. Tantot, H. Jallageas, G. E. Ponchak, M. M. Tentzeris, J. Papapolymerou, Characterization of liquid crystal polymer (LCP) material and trans- mission lines on LCP substrates from 30 to 110 GHz, IEEE T. Micro. Theory. 52 (2004) 1343-1352.